Available online at www.sciencedirect.com

SCIENCE DIRECT®

Surface Science 559 (2004) L173–L179

SURFACE SCIENCE

www.elsevier.com/locate/susc

Surface Science Letters

Heteroepitaxial growth of novel MoO_3 nanostructures on Au(1 1 1)

Monika M. Biener [a,b], Cynthia M. Friend [a,b,*]

[a] Department of Chemistry, Harvard University, 12 Oxford Street, Cambridge, MA 02138, USA
[b] Division of Engineering and Applied Sciences, Harvard University, 12 Oxford Street, Cambridge, MA 02138, USA

Received 10 February 2004; accepted for publication 16 April 2004
Available online 10 May 2004

Abstract

We have developed a synthetic procedure that yields novel nanocrystalline, islands of MoO_3 on Au(1 1 1). Careful control of the growth conditions yields monolayer islands with a rectangular unit cell that is aligned with the Au substrate. These structures are distinctly different than either bulk MoO_3 or than ramified, two-dimensional MoO_3 islands formed on Au(1 1 1) which were recently reported [J. Am. Chem. Soc. 125 (2003) 8059, Surf. Sci. 512 (2002) L353]. The atomic structure of these single-layer MoO_3 islands has been characterized by scanning tunnelling microscopy (STM), low energy electron diffraction (LEED), X-ray photoelectron spectroscopy (XPS), and Auger electron spectroscopy (AES). We discuss our synthetic method and important characteristics of the MoO_3 islands.

Keywords: Low energy electron diffraction (LEED); Scanning tunneling microscopy; Catalysis; Epitaxy; Growth; Surface chemical reaction; Gold; Molybdenum oxides

1. Introduction

Metal oxides are of considerable interest because of their electronic properties and their role in several important technologies. One significant application of metal oxides is in the area of heterogeneous catalysis, in particular conversion of hydrocarbons to oxygenates that is of interest as alternative fuels and as building blocks for other chemicals. Molybdenum trioxide is specifically known to promote the partial oxidation of methane to formaldehyde [3–6].

Metal oxides have a wide range of chemical, electronic and optical properties that depend on stoichiometry and size scale. For example, bulk MoO_3 is a semiconductor with a bandgap of 2.8 eV; however, states are introduced in the gap when point defects due to loss of oxygen are introduced [7]. Catalytic activity is often attributed to the presence of oxygen vacancies associated with edge sites of the material [8].

Chemical, electronic, and optical properties of materials can be influenced by changing the length scale from macroscopic to nanoscale particles or

---

[*] Corresponding author. Address: Department of Chemistry, Harvard University, 12 Oxford Street, Cambridge, MA 02138, USA. Tel.: +1-617-495-4052; fax: +1-617-496-8410.
E-mail address: cfriend@deas.harvard.edu (C.M. Friend).

doi:10.1016/j.susc.2004.04.021

films. For example gold nanoparticles dispersed on metal oxides are chemically active [2,9], whereas bulk gold is inert. Molybdenum clusters on gold exhibit a very low activity towards O_2 and CO [2,10], whereas bulk Mo dissociates CO and O_2 below 300 K [11,12], providing another example. Hence, it is important to develop methods for synthesizing nanoscopic materials.

In this work, we describe a procedure that yields novel nanocrystalline, monolayer islands of MoO_3 on Au(1 1 1). The possibility of creating well-defined, single layer MoO_3 nanocrystals is a first step towards the development of materials with unusual chemical and physical properties.

2. Experimental

All experiments were performed in an ultrahigh vacuum (UHV) system with a base pressure of 4×10^{-10} Torr. The system is equipped with a “beetle-type” STM and commercial instrumentation for AES and LEED, described elsewhere [13,14]. The sample was radiatively heated via a tungsten filament located behind the sample. The temperature was monitored by a chromel/alumel thermocouple affixed to the sample holder. To account for the temperature gradient of the sample holder versus the crystal a calibration was performed using a thermocouple directly mounted to the crystal.

The Au was cleaned by cycles of Ar^+ sputtering (1000 eV, $\sim$5 μA) at 300 K, followed by annealing to 700 K for 10 min and 600 K for 60 min. This procedure was repeated several times until no contaminants were detected using AES. Following this procedure, a LEED pattern characteristic of the Au(1 1 1)-($22\times\sqrt{3}$) reconstruction [15] was observed. The “herringbone” reconstruction was also observed by STM.

$Mo(CO)_6$ (Alfa Aesar) was initially purified by freeze–pump–thaw cycles, and NO_2 (Matheson, anhydrous grade) was used as received. Both reagents were introduced to the sample by backfilling the chamber to 1×10^{-7} Torr. Gas lines were evacuated before each dose. All exposures are given in uncorrected ion gauge readings using units of Langmuir (1 L $=10^{-6}$ Torr s).

Molybdenum nanoclusters were deposited on Au(1 1 1) surfaces at 450 K via chemical vapor deposition (CVD) of $Mo(CO)_6$. Nanocrystalline MoO_3 was prepared by subsequent exposure to NO_2 at 450 K, followed by annealing at 600 K.

All STM images were collected at room temperature using commercial $Pt_{0.8}Ir_{0.2}$ tips (molecular imaging). Scan dimensions were calibrated by imaging the unit cell of the Au(1 1 1) surface. The sample bias voltage was set between +0.1 and +2.8 V. All images are unfiltered and only background corrected.

3. Results and discussion

Preferential nucleation of three-dimensional molybdenum nanoclusters at step edges was observed after dosing 4 L of $Mo(CO)_6$ onto the Au(1 1 1)-($22\times\sqrt{3}$) surface maintained at 450 K (Fig. 1). The apparent height of the Mo clusters is in the range of 0.3–0.7 nm and their average diameter is $\sim$10 nm. No carbon or oxygen was detected by AES. The herringbone reconstruction persists on the terraces of the Au surface following deposition of the Mo clusters (data not shown).

The preferred nucleation of Mo clusters along the step edges is in contrast to the deposition of

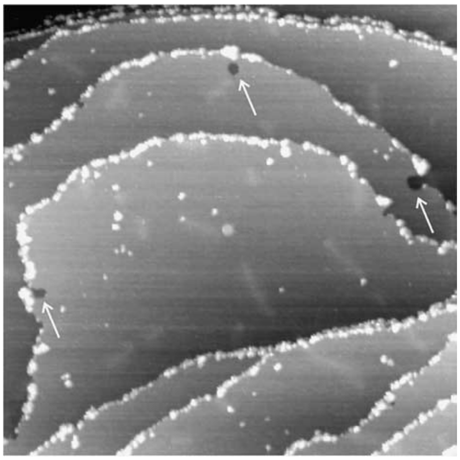

Fig. 1. STM image showing Mo particles formed by exposure of the Au(1 1 1)-($22\times\sqrt{3}$) surface to 4 L of $Mo(CO)_6$ at 450 K. Etch holes are indicated by arrows. The image was obtained at 300 K and corresponds to an area of 400 nm×400 nm.

Mo via physical vapor deposition (PVD), where the clusters preferentially nucleate at the elbow sites of the herringbone reconstruction as reported recently [16] and reproduced in our laboratory [17]. Our results are also different than those reported previously for growth of Mo clusters deposited using thermal decomposition of $Mo(CO)_6$, but using a different experimental configuration [18]. This difference is attributed to the strong sensitivity of the CVD process to temperature and to CO induced mobility of Mo nanoclusters [19].

The strong sensitivity of the CVD process to surface temperature is illustrated by the fact that the deposition rate decreases to an immeasurable rate at a surface temperature of 400 K. Specifically, no Mo was detected by means of STM after exposure of up to 100 L at 10^{-7} Torr of $Mo(CO)_6$ to the surface maintained at 400 K. Furthermore, no extraneous material or other changes were observed. This decrease in deposition rate is consistent with the fact that the CVD process is thermally activated. At minimum, dissociation of one Mo–CO bond is required to deposit Mo from $Mo(CO)_6$, which has an energy cost of $\sim$40 kcal/mol [20]. Surprisingly, the amount of Mo observed using STM after exposure of 4 L of $Mo(CO)_6$ to the Au surface maintained at 500 K was less than 20% of that observed at 450 K using the same flux and integrated dose. This observation is consistent with precursor-mediated decomposition: at higher temperatures the surface lifetime of the $Mo(CO)_6$ precursor decreases due to an increased desorption rate. The lifetime, τ, of the precursor would decrease by a factor of 5 upon increasing the surface temperature from 450 to 500 K. This estimate assumes a $Mo(CO)_6$ desorption barrier of 14 kcal/mol [18] and that the pre-exponential factor for desorption, A, is the same at the two temperatures. The ratio of lifetimes at the two temperatures is calculated using the Frenkel equation: $\tau = 1/A* \exp(E_{des}/RT_s)$, where E_{des} is the activation barrier and T_s is the surface temperature. The pre-exponential factors cancel in the ratio. This is in agreement with our observation that the Mo coverage decreased to $\sim$20%.

The Au surface itself promotes the decomposition of $Mo(CO)_6$ based on the fact that small sulfur coverages (<0.1 ML) completely inhibit the decomposition of $Mo(CO)_6$ on the Au(1 1 1) surface, most likely by poisoning active sites. Specifically, no Mo was detected after exposure to 4 L $Mo(CO)_6$ at 450 K by means of AES and STM. If the Au surface were simply a source of thermal energy, there would not be such a strong dependence of the Mo deposition rate on the presence of a small amount of impurity. It is known that the most stable bonding sites for sulfur are located at the step edges of Au(1 1 1) [21]. This indicates that the active sites for $Mo(CO)_6$ decomposition are related to step edges of the Au surface. We were, however, not able to identify the active sites by STM.

The Mo nanoclusters probably also contain Au based on changes in the surface morphology observed in STM following CVD of the Mo. Specifically, the originally straight step edges become irregular. Etch holes appear along the step edges between neighbouring molybdenum clusters (Fig. 1). These observations are also consistent with the appearance of nanoscopic holes as observed in our previous work [19] when Mo is transported from terraces to step edges by CO exposure.

Oxidation of the Mo nanoclusters using exposure to NO_2 at 450 K leads to spreading into a two-dimensional layer and full oxidation to MoO_3, in qualitative agreement with previous studies [1,2]. The predominant oxidation state was determined to be Mo^{6+} using X-ray photoelectron spectroscopy (data not shown), as described in detail elsewhere [22].

Nanocrystalline MoO_3 islands that are one layer high and ordered relative to the underlying gold surface are formed using our iterative dosing procedure described below (Figs. 2 and 3). The structure of the observed single-layer MoO_3 differs from the bilayer structure of bulk MoO_3 [23] and can be explained in terms of an ordered, two-dimensional array of interacting MoO_3 entities based on a combination of experimental data and associated density functional theory calculations, described elsewhere [24]. The apparent height of the islands is $\sim$0.5 nm, in contrast to 1.38 nm as the height of a bulk bilayer unit cell, which is consistent with the single layer structure described above.

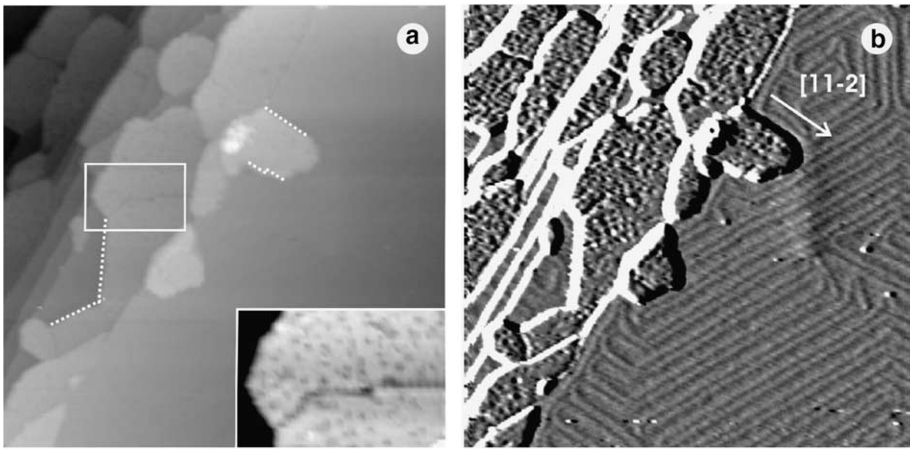

Fig. 2. STM image showing nanocrystalline MoO_3 islands on Au(1 1 1) after alternate exposure to 1 L $Mo(CO)_6$ and 10 L NO_2 at 450 K followed by annealing to 600 K for 1 min after every four cycles of dosing for a total of 16 cycles: (a) alignment of the island edges (dotted lines) with the ⟨1 1 −2⟩ directions of the substrate: a magnification of a domain wall is shown in the inset (28 nm × 18 nm); (b) image is differentiated to enhance the contrast and show the orientation of the substrate. The ⟨1 1 −2⟩ directions run parallel to the herringbone dislocation lines; one of them is indicated in the figure. The total coverage, as estimated by AES, is ~0.3 ML, however, the local coverage is strongly dependent on the substrate step density. The image was obtained at 300 K and corresponds to an area of 120 nm × 120 nm.

The MoO_3 islands nucleate preferentially along step-edges, and exhibit well-defined edges with kinks and domain walls (Fig. 2). The islands are aligned with the Au(1 1 1) surface, based on the observation of a well-ordered LEED pattern (see Fig. 3c and discussion below). STM reveals that the island edges run parallel to the ⟨1 1 −2⟩ directions of the substrate, if the shape of the islands is not dictated by the step edges of the substrate. STM data further reveal a rectangular unit cell with dimensions of 0.50×0.57 $nm^2 \pm 10\%$, consistent with the observation of a well-defined c(2 × 4) LEED pattern (Fig. 3). Note that the observation of the c(4 × 2) LEED pattern, as shown in (Fig. 3c), implies the existence of rotational domains. Occasionally, domain walls (Fig. 2a, inset) were observed by STM. The growth of the MoO_3 islands away from the step edge is a direct consequence of the fact that the Mo clusters have nucleated at the step edge prior to oxidation. Nanocrystalline MoO_3 islands with the same unit cell form on terraces when Mo clusters, deposited using physical vapor deposition, are oxidized [17]. The alignment of those islands with the Au substrate is more pronounced, compared to the islands shown in (Fig. 2), as the island shape is not dictated by the Au step edges.

The crystallinity of the MoO_3 islands depends on the conditions used for oxidation due to kinetic control of the oxidation and growth. Small Mo clusters (diameter $\leqslant 5$ nm) are required as starting material in order to form crystalline structures. Disordered molybdenum oxide particles, which are only partially oxidized to Mo + 6 and not completely spread into small 2D islands, form upon oxidation of larger Mo clusters (Fig. 4). In order to grow large MoO_3 islands, repeated cycles of Mo deposition in small amounts and subsequent oxidation are used (Fig. 2). For example, the MoO_3 islands shown in Fig. 2 are formed by alternate exposure of the surface to 1 L of $Mo(CO)_6$ and 10 L NO_2 at 450 K followed by annealing to 600 K for 1 min after every four cycles of dosing for a total of 16 cycles. This procedure yields well-ordered islands with an average size of 600 nm^2—large enough to observe a clear LEED pattern.

In order to study the growth mechanism of the MoO_3 islands, $Mo(CO)_6$ was dosed at 450 K to a MoO_3-covered Au(1 1 1) surface. STM images

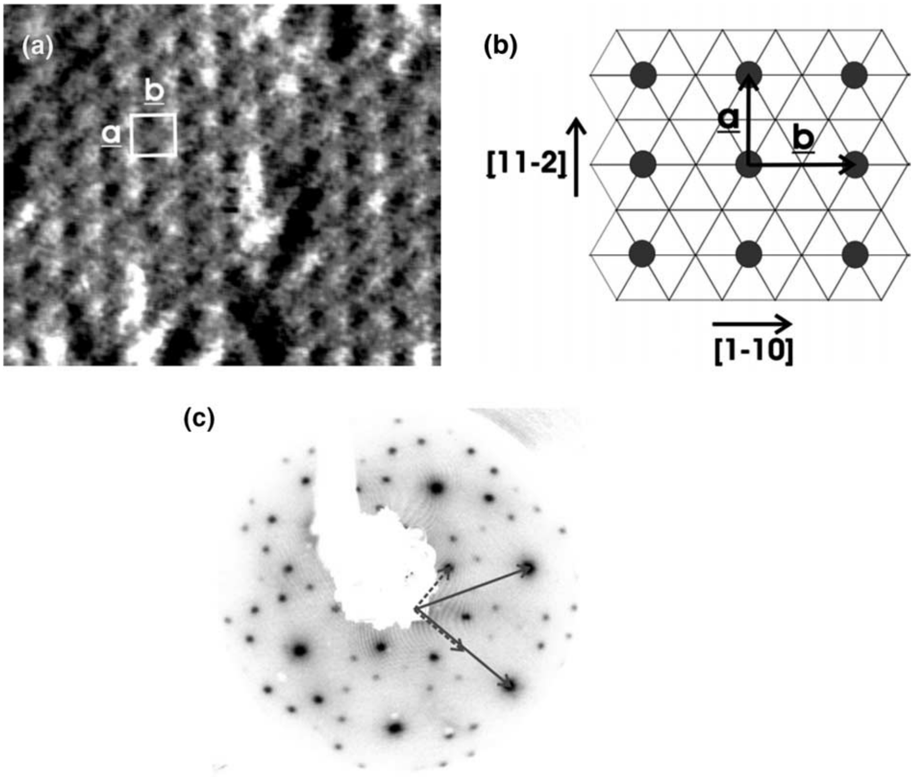

Fig. 3. Identification of the c(4×2) unit cell of the MoO_3 islands on Au(1 1 1) prepared by alternate exposure of the surface to 1 L $Mo(CO)_6$ and 10 L NO_2 at 450 K followed by annealing to 600 K for 1 min after every four cycles of dosing for a total of 16 cycles: (a) high resolution STM image (50 nm×60 nm) showing a rectangular unit cell with $a = 0.50$ nm and $b = 0.57$ nm ±10%, obtained at 300 K; (b) schematic of a c(4×2) superlattice on a hexagonal substrate, corresponding to unit cell dimensions of $a = 0.499$ nm, $b = 0.576$ nm for a Au(1 1 1) surface with the closest-packed rows of the superlattice running in the [1 1 −2] direction; (c) LEED pattern obtained at 300 K showing a c(4×2) structure (part of the picture is blocked out by the sample holder). Straight arrows indicate the basis of the hexagonal unit cell of the Au substrate, dotted arrows indicate the basis of one rotational domain (basis of the other two domains not shown) of the c(4×2) superlattice.

obtained at 300 K reveal that Mo clusters nucleate exclusively at Au step edges (Fig. 5). Mo deposition at edges of the MoO_3 islands was *not* observed. This implies that the oxidation of molybdenum clusters leads to mass transport from the step edges to the islands. Mobile MoO_3 species are created at the step edges and diffuse along the surface until they hit the edge of a MoO_3 island. Volatile $(MoO_3)_n$ ($n = 3$, 4, 5) species have been previously detected by mass spectrometric studies during sublimation of MoO_3 bulk oxide [25]. The compact shape of the islands indicates that the aggregation of these mobile clusters is reversible [26]. Detachment from the island or diffusion along the edge of the islands is possible at the chosen temperature (450 K) and influences island shape and size. Larger crystalline islands grow at the expense of smaller islands. Small islands have a larger perimeter to area ratio than large islands and are thus thermodynamically less favorable (Ostwald ripening). In contrast, a fractal island shape can be expected if the substrate temperature is too low to activate detachment of atoms or clusters from the islands and thus aggregation is irreversible [26].

Gold as a noble metal is ideally suited as inert support for the oxidation of metals since neither O_2 nor NO_2 decompose under UHV conditions on

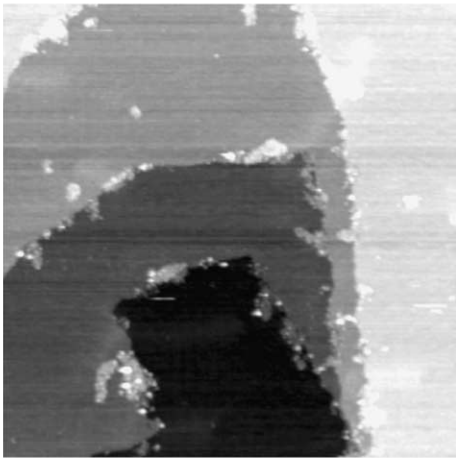

Fig. 4. STM image showing partially oxidized Mo oxide islands formed by exposure of 4 L of $Mo(CO)_6$ and 40 L of NO_2 at 450 K. The image was obtained at 300 K and corresponds to an area of 200 nm × 200 nm.

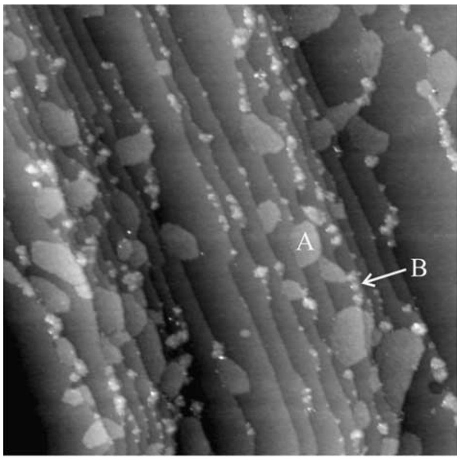

Fig. 5. STM image showing a MoO_3-covered Au(1 1 1) surface after exposure to 1 L of $Mo(CO)_6$ at 450 K. The figure illustrates that Mo clusters (B) nucleate exclusively at Au step edges and not at the edges of the MoO_3 islands (A). The image was obtained at 300 K and corresponds to an area of 300 nm × 300 nm.

Au(1 1 1) [27,28]. Selective oxidation of metal clusters deposited on Au(1 1 1) is, thus, possible by exposure to an oxidant. Recently the inertness of Au(1 1 1) was utilized to grow V_2O_3 films by evaporation of vanadium in an oxygen atmosphere [29]. The weak interaction of Au with oxygen also facilitates the diffusion of the MoO_3 species. However, the interaction is strong enough to influence the structure and orientation of the MoO_3 islands. As Mo has a higher surface free energy (2.88 $J\,m^{-2}$) than gold (1.62 $J\,m^{-2}$) [30] the formation of 3D molybdenum nanoclusters can be expected. The spreading of the 3D metal clusters during oxidation is consistent with the low free surface energy of MoO_3 ($5–7\times10^{-2}$ $J\,m^{-2}$) [31].

4. Conclusion

We are able to grow two-dimensional compact MoO_3 islands on Au(1 1 1) by carefully controlling the growth kinetics. A c(4×2) unit cell was determined by STM and LEED. The location of the deposited metal clusters dictates the initial nucleation sites for the metal oxide islands. Repeated cycles of Mo cluster deposition and oxidation in small increments are necessary to create mobile MoO_3 species that are responsible for the mass transport and thus for the island growth. The possibility to create well-defined nanocrystalline MoO_3 islands will enable the study of interesting reactions that are relevant in the field of catalysis and novel sensors. Furthermore, we expect that this methodology can be generalized to the growth of other nanoscopic metal oxides.

Acknowledgements

We gratefully acknowledge support of this work by the National Science Foundation under support for the Harvard Nanoscale Science and Engineering Center, grant no. PHY-011-7795, and the Department of Energy, Basic Energy Sciences, FG02-84-ER13289.

References

[1] Z. Song, T. Cai, Z. Chang, G. Liu, J.A. Rodriguez, J. Hrbek, J. Am. Chem. Soc. 125 (2003) 8059.
[2] Z.P. Chang, Z. Song, G. Liu, J.A. Rodriguez, J. Hrbek, Surf. Sci. 512 (2002) L353.
[3] P.J. Spencer, United States Patent 4,607,127 (1986).
[4] N.D. Spencer, C.J. Pereira, AIChE J. 33 (1987) 1808.

[5] N.D. Spencer, J. Catal. 109 (1988) 187.
[6] M.A. Banares, N.D. Spencer, M.D. Jones, I.E. Wachs, J. Catal. 146 (1994) 204.
[7] M. Chen, C.M. Friend, E. Kaxiras, JACS (2001).
[8] J. Haber, E. Lalik, Catal. Today 33 (1997) 119.
[9] M. Valden, X. Lai, D.W. Goodman, Science 281 (1998) 1647.
[10] J.A. Rodriguez, J. Dvorak, T. Jirsak, J. Hrbek, Surf. Sci. 490 (2001) 315.
[11] A.J. Jaworowski, M. Smedh, M. Borg, A. Sandell, A. Beutler, S.L. Sorensen, E. Lundgreen, J.N. Andersen, Surf. Sci. 492 (2001) 185.
[12] G.H. Smudde, P.C. Stair, Surf. Sci. 317 (1994) 65.
[13] P.G. Clark, C.M. Friend, J. Chem. Phys. 111 (1999) 6991.
[14] M. Chen, P.G. Clark, T. Mueller, C.M. Friend, E. Kaxiras, Phys. Rev. B 60 (1999) 11783.
[15] M.V.R. Murty, T. Curcic, A. Judy, B.H. Cooper, Phys. Rev. B 60 (1999) 16956.
[16] S. Helveg, J.V. Lauritsen, E. Laegsgaard, I. Stensgaard, J.K. Norskov, B.S. Clausen, H. Topsoe, F. Besenbacher, Phys. Rev. Lett. 84 (2000) 951.
[17] M.M. Biener, J. Biener, R. Schalek, C.M. Friend, in press.
[18] Z. Song, T.H. Cai, J.A. Rodriguez, J. Hrbek, A.S.Y. Chan, C.M. Friend, J. Phys. Chem. B 107 (2003) 1036.
[19] A. Chan, B. Richter, C. Friend, M. Aziz, J. Hrbek, Z. Song, Nano Letters (2003).
[20] K.E. Lewis, D.M. Golden, G.P. Smith, J. Am. Chem. Soc. 106 (1984) 3912.
[21] C. Vericat, J.N. Andersen, M.E. Vela, R.C. Salvarezza, J. Phys. Chem. B 104 (2000) 302.
[22] M.M. Biener, J. Biener, X. Deng, C.M. Friend, in press.
[23] E. Itoh, K. Hayakawa, S. Oishi, J. Phys.: Condens. Matter 13 (2001) 6853.
[24] S.Y. Quek, M.M. Biener, J. Biener, C.M. Friend, E. Kaxiras, in press.
[25] G. Demaria, R.P. Burns, J. Drowart, M.G. Inghram, J. Chem. Phys. 32 (1960) 1373.
[26] A.-L. Barabasi, H.E. Stanley, Fractal Concepts in Surface Growth, Cambridge University Press, Cambridge, 1995.
[27] J. Wang, E. Koehl, J. Phys. Chem. A 102 (1998) 8573.
[28] N.D.S. Canning, D. Outka, R.J. Madix, Surf. Sci. 141 (1984) 240.
[29] A.C. Dupuis, M. Abu Haija, B. Richter, H. Kuhlenbeck, H.J. Freund, Surf. Sci. 539 (2003) 99.
[30] L.Z. Mezey, J. Giber, Jpn. J. Appl. Phys. 21 (1982) 1569.
[31] C.B. Wang, C.T.H.E. Wachs, Langmuir 15 (1999) 1223.